REHABILITATION OF THE MUD MOUNTAIN BYPASS TUNNEL INVERT*

Christian AUEL
Project Engineer, DTK Member,
ILF CONSULTING ENGINEERS AUSTRIA GMBH

John R. THENE
Project Manager, ILF CONSULTING ENGINEERS AUSTRIA GMBH

AUSTRIA

James CARROLL
Project Manager, ILF CONSULTANTS, INC.

Chuck HOLMES
Staff Engineer, ILF CONSULTANTS, INC.

USA

Robert M. BOES
Director, Laboratory of Hydraulics, Hydrology and Glaciology, ETH ZURICH

SWITZERLAND

SUMMARY

This paper describes the design of the new tunnel invert lining of the 9-foot tunnel at Mud Mountain Dam, Washington, USA. The tunnel diverts all bed load sediments into the tailwater. Major invert abrasion has been observed in the existing steel lining. The new invert design consists of 0.59 m² and 0.79 m² granite

_____

* *Réhabilitation du radier de la galerie de dérivation des sédiments Mud Mountain*

blocks that are 0.25 m thick and placed tightly together along the tunnel. Stability analysis showed factors of safety ranging from 1.2 to 2.6 against uplift. This will be achieved with strip drains placed in the bedding material along the tunnel. A service-design-life analysis was performed using abrasion prediction modelling. This model was based on abrasion measurement data acquired from granite field tests at Pfaffensprung sediment bypass tunnel, Switzerland. The estimated annual abrasion depths for the granite were approximately 0.50 mm/year for average sediment transport conditions.

RÉSUMÉ

Cette publication décrit la conception du nouveau revêtement du radier du tunnel « 9-foot » du Barrage de Mud Mountain, Etat de Washington, USA. Le tunnel évacue toute la charge sédimentaire vers l'aval du barrage. Une abrasion massive du radier a été observée dans le revêtement en acier existant. Le nouveau dimensionnement du radier prévoit la pose de blocs de granit d'une surface de 0.59 m^2 à 0.79 m^2 et d'une épaisseur de 0.25 m scellés de manière étanche le long du tunnel. Une analyse de stabilité au soulèvement a démontré des facteurs de sécurité compris entre 1.2 et 2.6 vis-à-vis du soulèvement. Ces valeurs peuvent être atteintes avec des bandes drainantes placées dans le matériau du lit de pose le long du tunnel. Une analyse de la durée de vie en fonction des contraintes de service et de la conception a été menée en utilisant un modèle de prédiction de l'abrasion. Ce modèle est basé sur les données d'abrasion collectées lors d'essais in situ dans le chenal de déviation des sédiments du tunnel de Pfaffensprung en Suisse. Les profondeurs d'abrasion annuelles estimées pour le granit étaient d'environ 0.50 mm/an pour un transport solide en conditions moyennes.

1.   INTRODUCTION

Mud Mountain Dam is a 132 m high flood retention dam completed in 1948 and operated by the U.S. Army Corps of Engineers, Seattle District (Fig. 1a). The dam controls floods on the White River, a gravel bed river originating from the northern slope of Mt. Rainier, a 4392 m high active volcano in western Washington State, USA.

Two tunnels, referred to by their widths of 23 ft (7.0 m) and 9 ft (2.74 m), drain the reservoir. The upstream invert of the 9-ft tunnel (termed NFT hereafter) is at elevation (El.) 271 m, while the 23-foot tunnel intake is at a higher elevation (Fig. 1b). The overflow spillway crest is at El. 370 m.
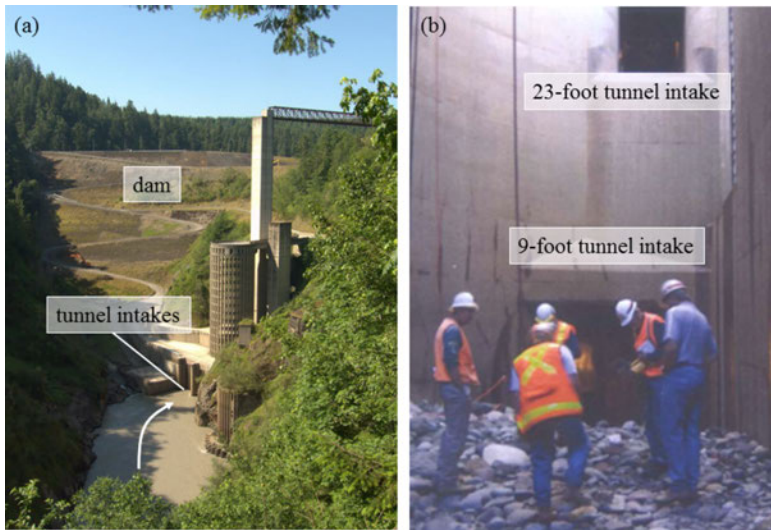
Fig. 1
Photographs of a) Mud Mountain dam and tunnel intake structures in 2012
(courtesy of Mike Betz), b) tunnel intakes with sediment deposition [1].
*Photographies a) du barrage de Mud Mountain et du tunnel d'amenée en 2012
(courtoisie Mike Betz) b) des prises dans le tunnel d'amenée avec dépôts de
sédiments [1].*

The NFT is opened three to four times per year in order to pass sediment through the dam that has accumulated in the reservoir. The river flows are normally diverted via the 23 ft tunnel. During floods, the NFT is operated for reservoir levels up to El. 283.5 m, but it will be operated up to El. 295.7 m after relining the invert. The tunnel is closed at higher reservoir levels, while the 23-foot tunnel remains open [1]. Because of the elevation difference between the two tunnels, the 23 ft tunnel only passes suspended sediment while the NFT passes suspended sediment and bed load sediment. The NFT is 505 m long, the invert slope is S_b = 0.0194, and the cross section is of archway type. In 1995, a 2.5 cm-thick planar steel lining was placed in the invert; it extends vertically to armor the lower sidewalls.

The annual average sediment load entering the reservoir is about 450,000 tons, of which the bed load is about 11%. Thus Q_s = 49,500 tons/year are bypassed with a standard deviation of ±62%, representing wet years with many floods and dry years with rather low flow conditions, respectively [2]. The median sediment particle diameter D_{50} upstream of the reservoir is 62 mm. The bedload sediment has been quite destructive, and significant abrasion of the steel lining occurred over its entire width. The most wear occurred where secondary flow currents

naturally concentrate the bed load, wearing through the 2.5 cm steel lining locally after only 12 years of operation (Fig. 2a). The underlying reinforced concrete has also experienced significant scour losses in locations where the protective steel lining had been worn through (Fig. 2b).

Fig. 2
Abrasion patterns in the steel lining of Mud Mountain NFT. Photograph in a) 2015: longitudinal abrasion channel along the sidewall [1], b) 2007: damage extended into the concrete lining below the steel plate.
Effets de l'érosion sur le revêtement en acier du NFT de Mud Mountain –
photographies de a) chenal d'abrasion le long d'un mur latéral du NFT (2015) [1],
b) dommages étendus jusqu'au béton sous une plaque d'acier (2007).

The US Army Corps of Engineers tendered the rehabilitation of the tunnel invert, which was awarded to and carried out by the Design-Builder Garney Construction who was supported by the Design-Consultant ILF Consultants, Inc. This paper describes (1) the new tunnel invert lining design, (2) the stability analysis of the invert lining, and (3) the predicted invert abrasion ([3], [4]).

2.   TUNNEL INVERT DESIGN

2.1.   CONCEPT

The concept for the proposed invert design is based on the high abrasion resistance of hard natural stone. Its abrasion resistance has been proven over decades of use in the lining of hydraulic structures in sediment bearing streams. The Pfaffensprung sediment bypass tunnel (hereafter SBT) in Switzerland, a recent and well-documented project utilizing a granite lining, was available to provide a substantial basis for the design of the NFT invert lining [5]. Pfaffensprung experiences flow and bed load characteristics similar to those of Mud Mountain (Table 1).

Table 1

Characteristics of Mud Mountain NFT and Pfaffensprung SBT

FACILITY	TUNNEL LENGTH	FLOW AREA	SLOPE	DESIGN DISCHARGE	MAXIMUM FLOW VELOCITY	TOTAL SEDIMENT INFLOW	BED LOAD SEDIMENT INFLOW	MEDIAN SEDIMENT DIAMETER	DAYS OPENED
	[M]	[M²]	[%]	[M³/S]	[M/S]	[M³/YEAR]	[M³/YEAR]	[MM]	[DAYS/ YEAR]
Pfaffensprung	282	18.5	3.0	220	15	264,000	132,000	250	100-200
Mud Mountain	505	5.1	1.94	70	11	170,000*	18,700*	62	10-25

*originally given in tons, divided by 2.65 t/m³, Pfaffensprung data from [6].

The average bed load moving through Pfaffensprung is 132,000 m³/year. The tunnel invert at Pfaffensprung consists of 1.0 m square granite blocks which are 30 cm thick (Fig. 3). The precision-cut blocks (accuracy ± 2 mm) were placed in direct contact with each other without mortar or other material in the joints; longitudinal joints were staggered. The blocks were set in a thin mortar bedding on top of a planar layer of drainage concrete. The gaps between the tunnel walls and the pavement were filled with cast basalt tiles and abrasion-resistant mortar. A longitudinal drainage pipe is placed in the drainage concrete at the centerline of the tunnel and daylights at the tunnel exit.

Fig. 3
Photographs of Pfaffensprung SBT. a) Granite block placement, b) finished tunnel invert (courtesy of VAW, ETH Zurich) [3].
Photographies du chenal de déviation des sédiments du tunnel de Pfaffensprung. a) positionnement d'un bloc de granit b) radier du tunnel terminé (courtoisie VAW, ETH Zurich) [3].

2.2.   NFT INVERT DESIGN

Like the Pfaffensprung SBT, the new invert design of the NFT consists of two primary components, a subgrade and a wear surface. The subgrade is prepared with a layer of pervious concrete placed on the existing steel invert and installed strip drains. The new wear surface consists of precision-cut, tight-fitting granite blocks with abrasion-resistant concrete filling the gap between the granite blocks and the tunnel walls (Fig. 4).

Optical scanning technology was used to create a 3D model of the existing tunnel. This was done to aid in the design of the precision cut granite and to ensure that there would not be interference between the granite blocks and

the tunnel wall. A 2D model of the design section (Fig. 4) was projected along the length of the 3D tunnel model to identify any conflicts. As shown in Fig. 5, intersections between the granite blocks (white outline) and the tunnel wall were identified in red, while green denoted no conflict.
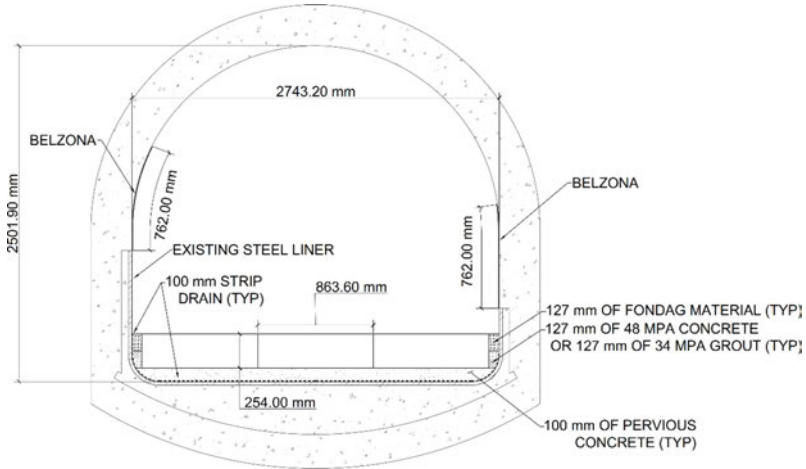

Fig. 4
Typical NFT Cross Section.
Section transversale type du NFT.

2.3.   PERVIOUS CONCRETE SUBGRADE

Pervious concrete was selected for the subgrade in order to disperse any local inflows to the subgrade and prevent the build-up of pressure under the granite blocks (Section 3.5). Pervious concrete will allow water flow through the subgrade and into the strip drains (Section 2.4). To make pervious concrete, gravel material is mixed with light amounts of cement, resulting in a porous, permeable matrix. The pervious concrete will be transported into the tunnel by electric bug-gies and placed by hand screeding.
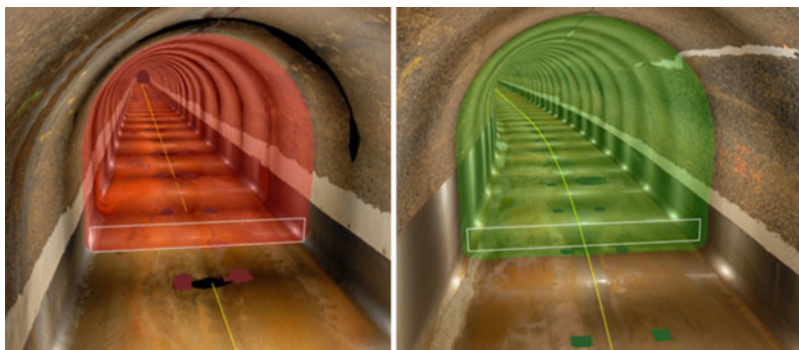
Fig. 5
Photographs of a tunnel cross section incl. 3D LiDAR data and a 2D model
(white outline) of the proposed granite invert design. Green indicates no conflict
between tunnel wall and invert block, red indicates a conflict.
*Photographie d'une section transversale du tunnel avec données LIDAR 3D et un
modèle 2D (rectangle blanc) du radier en granit proposé. La couleur verte indique
l'absence de conflit entre les parois du tunnel et les blocs de granit, le rouge
l'existence d'un tel conflit.*

2.4.   SUBGRADE STRIP DRAINS

Subgrade strip drains are embedded within the pervious concrete at approxi-
mately 7.6 m intervals, and they extend to the granite block surface at both
sidewalls. These strip drains remove excess water from the subgrade and prevent
pressure build-up beneath the granite blocks. Water is conducted through the open
plastic inner core which is protected from clogging by a sleeve of geotextile filter
fabric. It is anticipated that discharge from the strip drains will prevent sediment
infiltration. The permeability of the strip drain is higher than that of the pervious
concrete creating a path of least resistance that will facilitate the removal of
water from the subbase.

2.5.   GRANITE BLOCKS

The *Hardy Island Granite* blocks were cut and finished at the quarry and
delivered to the project site in the required configurations. All blocks are 25 cm
thick and 91 cm long in the flow direction, while the standard widths are 65 cm
and 86 cm (Fig. 6). The dimensional tolerance for the block length is ±1.6 mm,
while for the block thickness and width it is ±3.2 mm. Truncated-wedge shapes
were produced for the curved sections of the tunnel.

The blocks are to be placed in tight physical contact with one-another. In exceptional cases, the maximum allowable joint spacing for both the longitudinal and transverse joints is 6.4 mm. The 65 cm wide blocks make up the four-block row configuration, and the 86 cm wide blocks make up the three-block row configuration. Alternating rows of three and four blocks ensure offset longitudinal joints through the entire tunnel length.
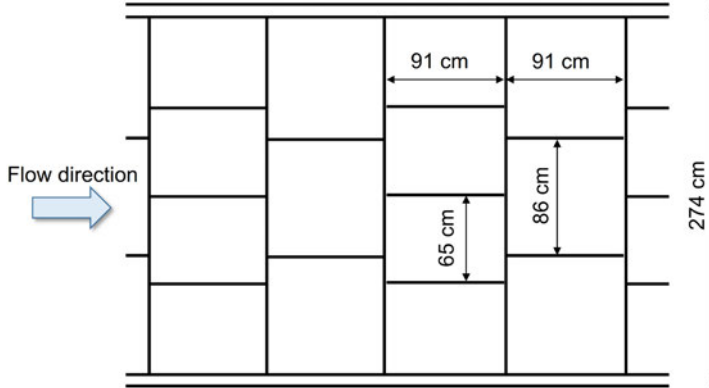

Fig. 6
Typical layout of granite blocks in the tunnel.
Schéma de pose type des blocs de granit dans le tunnel.

3.   STABILITY ANALYSIS

3.1.   GENERAL

Stability analysis of the blocks was undertaken to evaluate the potential stabilizing and destabilizing effects of the subgrade drainage layer due to the water moving through the gaps in the blocks. The results were used to identify potential hazards and test the effect of drainage and other measures to prevent destabilizing conditions. Assumptions made in the stability calculations are generally conservative, such as neglecting sliding friction between the blocks.

Static analysis of individual blocks was performed, taking into account the hydraulic loads acting on the blocks and the interaction of blocks within the tunnel. The analysis addresses blocks in the center of the tunnel, as they do not experience the additional resistance of the edge concrete. Two models were used to estimate hydraulic pressure acting on the blocks: (1) a 1D HEC-RAS model to simulate the hydraulics of the tunnel operation, and (2) a mathematical

model created to estimate the pressure head in the subgrade drainage system. After determining the pressures, loads were generated for each row of granite blocks. The existing steel invert prevents interaction with the groundwater outside the tunnel.

3.2.   TUNNEL HYDRAULICS AND DOWNWARD FORCES

The 1D HEC-RAS model was used to calculate the hydraulic head, average flow velocity, and bed shear stress. Three flow rates were considered (Table 2). Prior to rehabilitation, the pool limit was at Water Surface Elevation (WSEI) 283.5 m, while it will be raised to 295.7 m after relining the invert. The NFT is only operated with the radial gate fully open, so the flow rate is only dependent on the pool elevation. Operation (and hence stability and abrasion analysis) at pool elevations exceeding those in Table 2 were not considered, as the 23-foot tunnel is then operated exclusively.

Table 2
Discharges of Mud Mountain NFT [1]

FLOW RATE	USCS UNIT [FT/S]	SI UNIT [M³/S]	EXCEEDANCE [%]
Low Flow	1000	28	60
Intermediate Flow	2000	57	20
Flow at WSEI. 283.5 m	2400	68	13
Flow at WSEI. 295.7 m	2500	71	

The pressure head at the tunnel invert (energy head minus velocity head minus elevation) ranges from 2.23 m near the gate chamber to 1.04 m at the tunnel outlet at low flow (Fig. 7). Both the intermediate flow and the pool elevation conditions cause pressurized flow from the inlet nearly to the outlet, with maximum pressure heads up to 7.65 m and 16.03 m, for 57 and 71 m³/s respectively. The drop in the hydraulic grade line in the first 20 m downstream of the gate is due to a reduction in the flow area; the gradient over the remainder is due to friction.

3.3.   SUBGRADE PRESSURES AND UPLIFT FORCES

The pressures in the subgrade material – which also act on the bottom of the granite blocks – were calculated using a 1D finite element hydraulic model developed to track pressure and flow in the subgrade, as they are affected by flow through the vertical joints between blocks and the strip drains previously described. Both the longitudinal and traverse joints between blocks were considered in this model. The 1D subgrade model deals with flow rates several orders of magnitude smaller than the tunnel discharge rate. Therefore these flows did not influence the

flow in the tunnel, and the HEC-RAS model could be used to provide the upper boundary conditions on the blocks in terms of pressure and velocity (Fig. 8).
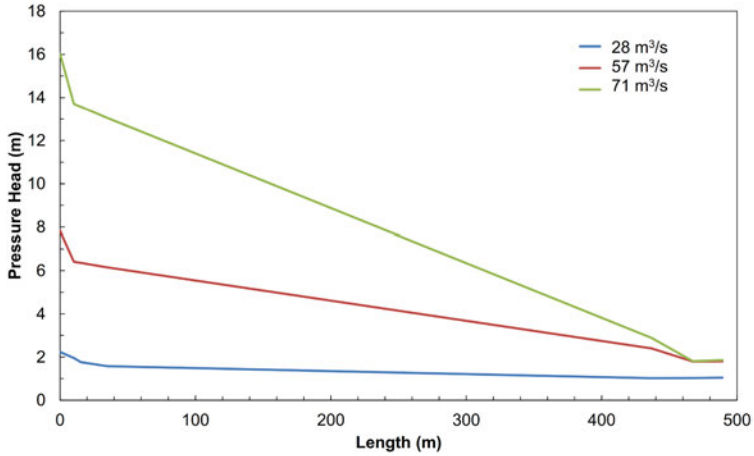

Fig. 7
Pressure head (above blocks) along the tunnel.
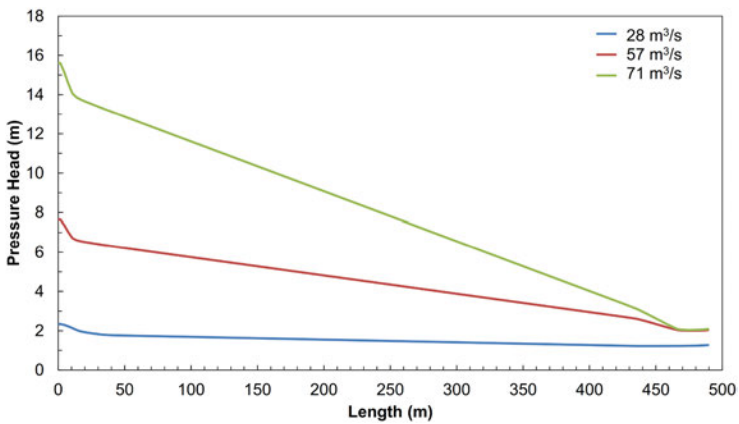*Profil des pressions (au dessus des blocs) le long du tunnel.*

Fig. 8
Uplift pressure (below blocks) along the tunnel (with sand filled joints).
Pression de soulèvement (sous les blocs) le long du tunnel (avec joints en sable).

In most of the tunnel, the gage pressure head (hydraulic head – elevation head) in the subgrade is larger than the gage pressure head above the blocks due to the difference in elevation (Fig. 9). However, the subgrade under the first few rows of granite blocks at the tunnel entrance has a lower gage pressure head under the blocks than above them. This is due to restricted access to the subgrade near the entrance of the tunnel, resulting in minimal water infiltration under the blocks. Thus pressure underneath those blocks is reduced. The peak differential pressure occurs due to the reduction in tunnel height from 2.74 m to 2.50 m. This reduced cross sectional area creates a change in the gradient of the pressure head above the blocks.
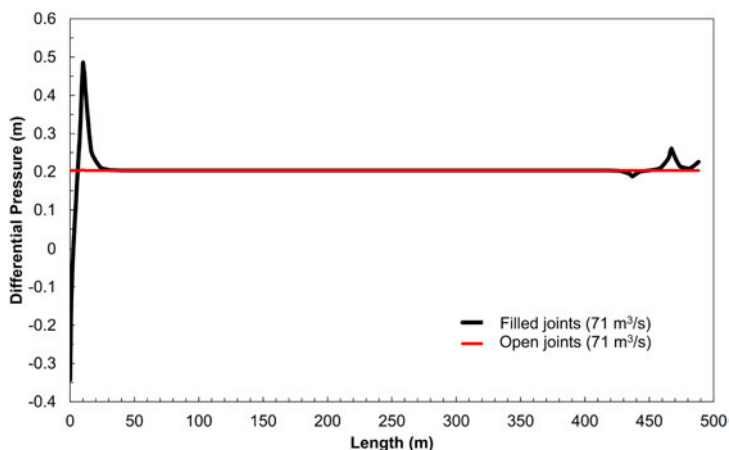

Fig. 9
Differential pressure along the tunnel at 71 m³/s for filled and open joints.
Pression différentielle le long du tunnel pour 71 m³/s dans le cas de joints pleins et ouverts.

3.4.   STAGNATION PRESSURE

Flowing water imparts lateral load on the invert blocks by two mechanisms: (1) surface friction on top of the block dependent on block roughness and water velocity, and (2) places where a vertical offset joint protruding into the flow blocks a small part of the flow and leads to stagnation pressure acting at the top of the joint. The transmission of this pressure downward into the joint and its effects on pressure and flow in the subgrade drive the primary destabilizing mechanism for stability against uplift.

Here, the stagnation pressure was determined using the average flow velocity and is equal to the velocity head at any point in the tunnel. The portion of the stagnation pressure acting at the top of the joint is determined based on empirical results measured by Frizell [7] (sealed arrangement). Actual velocities near the rock surface, and hence the stagnation pressure, will be smaller due to the boundary layer. The gaps between the blocks were assumed to be 3.2 mm and joint offsets were taken as 6.3 mm. The resulting empirical relation for the stagnation pressure P_{st} is as follows:

$$P_{st} = 0.00897U^{1.99619} \ \ [\text{ft}] \tag{1}$$

The calculated stagnation pressures were applied as a special case to the design criteria to investigate the sensitivity of each failure mode to offset joints between the granite blocks. The stagnation pressures act on the exposed offset surface protruding above the trailing edge of the upstream block thereby impeding downstream flow. Because the velocity is almost constant along the tunnel, there is little variation in the stagnation pressure aside from the entrance transition and the outlet where the flow cross sections vary.

Vertical offsets were assumed every second block row. The hydraulic head and the stagnation pressure were summed at locations with offset joints creating the boundary condition for the drainage calculations (Fig. 10). The stagnation pressure heads have a maximum of 5.90 m.

3.5.   UPLIFT ANALYSIS

The uplift stability safety factor was calculated as the block weight divided by the destabilizing force, which is the product of the net upward pressure and block area. The pressure head and the weight of block were the only downward-acting forces considered in the block stability analysis. Uplift was evaluated for individual blocks neglecting interaction (friction and normal forces) between blocks. If a block were to experience upward movement, new additional friction and normal forces (due to rotation) would resist further movement. Because uplift has fewer geometric constraints preventing failure than rotation, it was the focus of two investigations:

(1)   a design optimization study, where the uplift factors of safety (UFS) were the main design characteristics and the strip drain spacing was optimized, and

(2)   a sensitivity study where the uplift sensitivity of the system was determined based on the operational and hydraulic properties.
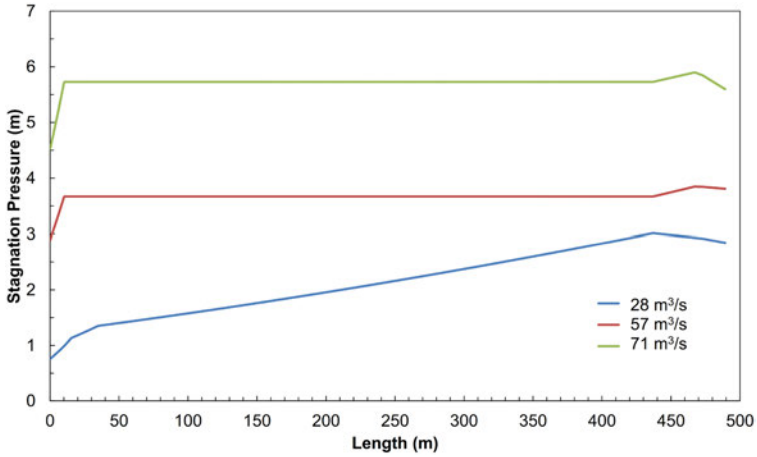
Fig. 10
Stagnation pressure along the tunnel for 6.3 mm vertical offset, and 3.2 mm gap.
Pressure only acts at vertical offset joints.
Pression d'arrêt le long du tunnel avec un décalage vertical de 6.3 mm et un espacement de 3.2 mm. La pression ne s'applique qu'aux joints avec décalage vertical.

The uplift factor of safety is determined as follows:

$$UFS = \frac{W}{\left(P_b - P_a\right)A}$$ [2]

where W = Weight of the block, P_b = Pressure on the bottom of the block, P_a = Pressure on the top of the block, A = Area of the block. The required Factor of Safety is minimum 1.2.

The differential pressure across the blocks varies along the tunnel due to changes in the geometry and hydraulic conductivity of the joints (see Fig. 9). To account for these changes, the strip drain spacing was determined individually for the different tunnel geometries. In Fig. 11, the resulting factor of safety is presented for different strip drain spacing along the alignment. Vertical offset joints were not assumed. For the tunnel section where the cross sectional area is constant, the factor of safety is 2.6.
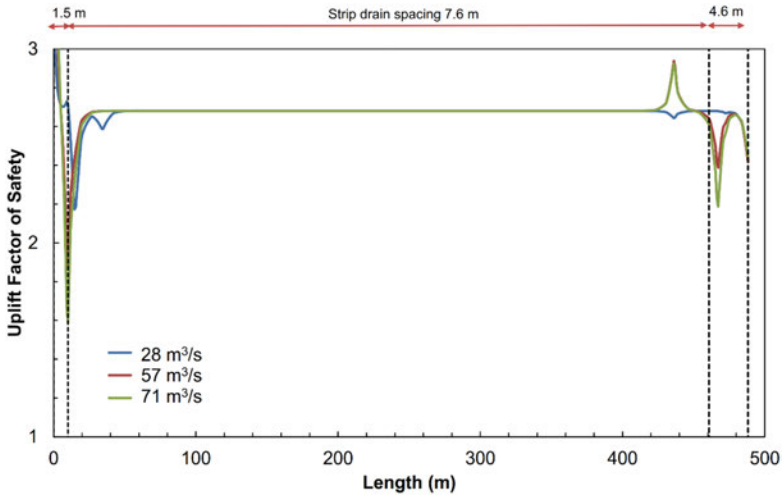
Fig. 11
Uplift factors of safety (UFS) along the tunnel for optimized strip drain spacing.
No vertical offsets assumed.
*Facteurs de sécurité au soulèvement (UFS) pour l'écartement optimal de la
bande drainante le long du tunnel.*

3.6.   UFS SENSITIVITY TO OFFSET HEIGHT AND FILLING CONDITION

Sensitivity analyses were performed with the maximum discharge of 71 m³/s
to analyze the variation of (1) offset height and (2) joint filling. Vertical offsets were
varied from 3.2 mm to 19 mm, while keeping the horizontal gap at 3.2 mm and
assuming sand filled joints (Fig. 12). The sand filled joints should be the normal
operational situation over the lifetime of the tunnel. The worst factor of safety is
associated with the largest vertical offset and improves as the offsets get smaller.
Furthermore, different joint filling conditions were analyzed assuming a constant
offset height of 6.3 mm (Fig. 13):

•   Condition 1 – Clean, open longitudinal and transverse joints: UFS < 1.0
     resulting in potential instability due to insufficient surface friction resistance.
•   Condition 2 – Sand-filled longitudinal and transverse joints with natural infill-
     ing: UFS   1.2, hence acceptable for all locations within the tunnel.
•   Condition 3 – Open longitudinal joints, sand filled transverse joints: Stagna-
     tion pressure only acts at the transverse joints, while pressure is allowed to
     dissipate from the longitudinal joints resulting in UFS   2.7.
•   Condition 4 – Sand-filled joints with no vertical offsets: UFS   2.7. This result
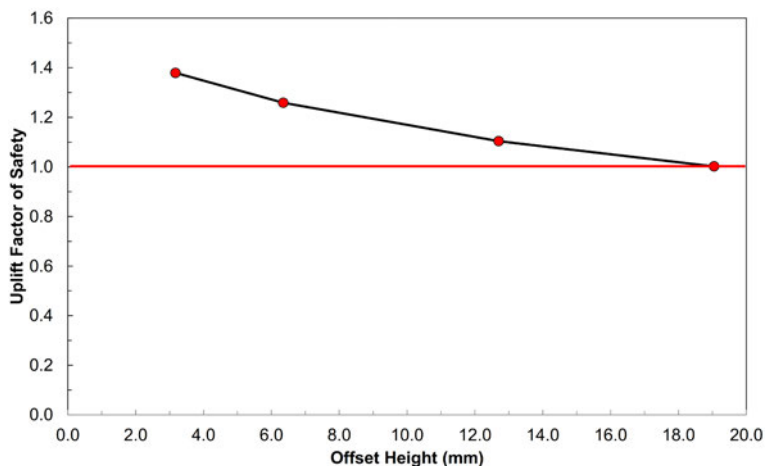   corresponds to the results in Fig. 11.

Fig. 12
UFS as a function of offset height for 71 m³/s. Sand filled joints assumed.
*Facteur de sécurité UFS en fonction du décalage vertical pour un débit de
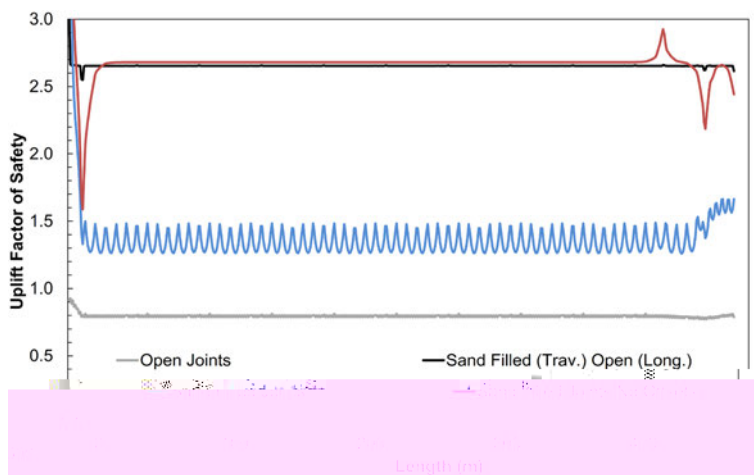71 m³/s et dans le cas de joints pleins en sable.*

Fig. 13
UFS along the tunnel for different joint fill conditions for 71 m³/s and vertical offset
height = 6.3 mm.
*Facteur de sécurité UFS le long du tunnel pour différents types de joint et pour un
débit de 71 m³/s et un décalage vertical de 6.3 mm.*

3.7.   RESULTING INVERT DESIGN SPECIFICATIONS

The final design of the blocks and details of their installation was informed by the stability calculations and sensitivity analysis described above. For an assumed vertical offset into the flow of 6.4 mm and with open joints, the sensitivity analysis indicated the need to prevent the transmission of stagnation pressures into the subgrade. Therefore, the design requires the joint to be modified to impede flow at least as effectively as the sand analyzed in Section 3.6 above. The specifications require that all transverse joints be blocked with a water-impeding material sandwiched between the rows of blocks. It was concluded that a flexible, adhesive sealant material applied at the time of construction would be acceptable in terms of performance and constructability. A bead of silicone-based caulk is to be used to seal the joints, though the contractor was given the option to present alternate materials for evaluation. Natural fine sediments will fill in the joints over time, reducing the dependency on the silicone caulk.

Furthermore, the maximum allowable offset into the flow is limited to 6.4 mm as included in the analysis. Observations from Pfaffensprung indicate that offsets into the flow are quickly abraded, thus limiting their effect on block stability. The tolerance for the gap between the blocks is 6.4 mm but it is specified that blocks be installed tightly.

Finally, the strip drain spacing will vary according to the results of the analysis to account for local pressure gradients caused by changes in cross section and flow velocity.

Similar to Pfaffensprung, the proposed invert lining of the NFT is expected to form a robust pavement that is resistant to potential forces acting upon it. This is supported by:

*   Precise geometric design combined with precision cutting and careful placement of the granite blocks, maximizing block to block contact and limiting the number and size of offsets into the flow;
*   A pervious subgrade for the dissipation of concentrated inflows;
*   Additional measures of a transverse joint sealant and strip drains to further reduce the potential for uplift;
*   Multiple conservative assumptions in the stability analysis; and
*   Self-correcting tendencies such as natural infilling of joints with fine sediments and abrasion of offsets protruding into the flow.

4.   ABRASION

Abrasion is a wear phenomenon involving progressive material loss due to hard particles impinging and sliding upon a solid surface. It is controlled by kinetic

energy due to the vertical component of saltating particles' impact (deformation wear) and by friction due to grinding stress (cutting wear) caused by the horizontal component [8], [9]. In general, abrasive damage can always be expected when particle bed load transport takes place. The governing process causing abrasion on brittle materials such as bedrock and concrete is saltation, whereas sliding and rolling do not cause significant wear [10], [11]. Cutting wear is more important for abrasion of steel, as in the existing invert design.

4.1.   ABRASION PREDICTION MODELS

Several mechanistic models exist to predict abrasion rates by taking the physical process of particle impact into account ([10], [12], [13]). They are derived from experimental research on particle motion characteristics, i.e. the analysis of particle impacts, velocities and saltation trajectories. Sklar and Dietrich developed a widely applied model for bedrock abrasion [10]:

$$A_r = 0.08g(s-1)\frac{Y_M}{k_v f_t^2} \cdot q_s \cdot \left(1 - \frac{q_s}{q_s^*}\right)\left(\frac{\theta}{\theta_c} - 1\right)^{-0.5}\left(1 - \left(\frac{U_*}{V_s}\right)^2\right)^{1.5} \quad [\text{m/s}] \qquad [3]$$

In this equation, Y_M = Young's Modulus of elasticity of the bed material [Pa], f_t = splitting tensile strength of the bed material [Pa], $k_v = 10^6$ = non-dimensional abrasion coefficient encompassing both the particle and bed material characteristics, q_s = bed load mass transport rate per unit width [kg/(sm)], and q_s^* = bed load mass transport capacity per unit width [kg/(sm)], U_* = $(gR_hS)^{0.5}$ = friction velocity, R_h = hydraulic radius, S = energy line slope for steady but gradually-varied flow, or bed slope for uniform flow, V_s = particle settling velocity, θ = Shields parameter calculated as θ = $U_*^2/[(s\,1)gD]$, s = ρ_s/ρ with ρ_s = particle density and ρ = fluid density, D = particle diameter, θ_c = critical Shields parameter. Auel proposed a revised version accounting for sub- and supercritical flows as well as fixed planar and alluvial beds ([12], [13]):

$$A_r = \frac{Y_M}{k_v f_t^2} \cdot \frac{(s-1)g}{230} q_s \left(1 - \frac{q_s}{q_s^*}\right) \quad [\text{m/s}] \qquad [4]$$

Based on the similarity between bedrock and concrete (both being brittle materials), a material strength-dependent Young's modulus formulation as well as a correlation of compressive to tensile strength was introduced [13]. Both the Young's modulus reformulation and new equations for vertical impact velocity and hop length led to an abrasion coefficient of $k_v = 10^5$, an order of magnitude lower than the values used in [10].

4.2.   SERVICE DESIGN LIFE - ABRASION PREDICTION

Abrasion calculations were performed based on the existing NFT dimensions for three different discharges as given in Table 2. Sediment transport took place only on 83 out of 365 days (23%) in 2011 [3]. Hence, it was concluded that bed load transport is only expected for river discharges larger than the intermediate flow, which was exceeded during 20% of the year (Table 2). In order to make abrasion calculations conservative, it was assumed that the NFT is always operated during bed load transport. A detailed description of these calculations is given in [3] and [4].

The estimated annual abrasion depths, A_d, for the granite invert of the Mud Mountain NFT varied from 0.34 mm/year (average) to 0.47 mm/year (severe) using Auel's model and from 0.15 mm/year (average) to 0.27 mm/year (severe) using the Sklar and Dietrich model. The lower abrasion depths from the latter model were attributed to the different data sets used to develop the models. The Sklar and Dietrich model was developed for incision in bedrock river beds where flow is subcritical and the bed is rough; the Auel model was developed for sub- to highly supercritical flow conditions and for bed configurations varying from planar to alluvial. Therefore, as a conservative estimate, the annual average depth of 0.47 mm/year or 0.26 mm per 10,000 tons of bed load per meter of tunnel width might be expected. This estimate is also supported by the results obtained at Pfaffensprung SBT in Switzerland [6]. Despite higher annual average abrasion depths of 2.9 mm/year, its rate per 10,000 tons/m of bed load was 0.26 mm and hence is the same as for Mud Mountain NFT. Although the granite for Mud Mountain NFT is stronger than the one at Pfaffensprung SBT (compressive strengths of 223 vs. 180 MPa), the different hydraulic conditions result in the same abrasion depth per 10,000 tons/m of bed load.

For long-term abrasion prediction, that is over decades, a spatially averaged annual abrasion depth of 0.47   0.50 mm/year $\pm85\%$ (estimation error resulting from uncertainty of k_v calculation at Pfaffensprung; [6]) for average sediment transport and 0.47×1.62 = 0.76   0.80 mm/year $\pm85\%$ for intense sediment transport conditions, respectively, should be considered as a conservative approach.

5.   CONCLUSIONS

ILF Consultants, Inc. proposed a new invert lining for the 9-foot tunnel at Mud Mountain dam. The tunnel is prone to high abrasion, as a large share of bed load sediment is transported through the tunnel. The new design consists of 0.59 m^2 or 0.79 m^2 large and 0.25 m thick granite blocks based on a similar design at Pfaffensprung bypass tunnel in Switzerland. Invert rehabilitation began in 2017.

ACKNOWLEDGEMENTS

REFERENCES

[1]   USACE. Mud Mountain Dam 9-Foot Tunnel Rearmoring, Enumclaw, WA - Construction Solicitation and Specifications, Phase 2 of 2. *US Army Corps of Engineers*, RFP No. W912DW-16-R-0006, 2016.

[2]   CZUBA, J.A., et al. Geomorphic analysis of the river response to sedimentation downstream of Mount Rainier, Washington. *U.S. Geological Survey Open-File Report* 2012-1242, 134p, 2012.

[3]   VAW. Mud Mountain Dam 9-foot Tunnel Re-armoring: Abrasion Calculations and Recommendations on the Invert Lining Concept - Expertise report. *VAW Report 4357*, Laboratory of Hydraulics, Hydrology and Glaciology, ETH Zurich, Switzerland, 2016.

[4]   Auel, C., Thene, J.R., Müller-Hagmann, M., Albayrak, I., Boes, R.M. Abrasion prediction at Mud Mountain sediment bypass tunnel. *Proc. 2nd Int. Workshop on Sediment Bypass Tunnels*, FP12, Kyoto, Japan, 2017.

[5]   MÜLLER, B., WALKER, M. The Pfaffensprung sediment bypass tunnel: 95 years of experience. *Proc. 1st Int. Workshop on Sediment Bypass Tunnels*, *VAW Mitteilungen* 232 (Boes, ed.), ETH Zurich, Switzerland, 247-258, 2015.

[6]   MÜLLER-HAGMANN, M. Hydroabrasion by high-speed sediment-laden flows in sediment bypass tunnels. *PhD Thesis 24291*, *VAW-Mitteilungen* 239 (R. Boes ed.), ETH Zurich, Switzerland, 2017.

[7]   FRIZELL KW. Uplift and crack flow resulting from high velocity discharges over open offset joints – Laboratory studies. *Report* DSO-07-07, US Bureau of Reclamation, Technical Service Center, Denver, Colorado, 2007.

[8]   BITTER, J.G.A. A study of erosion phenomena, part I. *Wear* (6): 5–21, 1963.

[9]   BITTER, J.G.A. A study of erosion phenomena, part II. *Wear* (6): 169–190, 1963.

[10] SKLAR, L.S., Dietrich, W.E. A mechanistic model for river incision into bed-rock by saltating bed load. *Water Resources Research* 40(W06301), 2004.

[11] TUROWSKI, J.M. Semi-alluvial channels and sediment-flux-driven bedrock erosion. *Gravel-Bed Rivers: Processes, Tools, Environments* (eds. M. Church, P. M. Biron and A. G. Roy), John Wiley & Sons, Ltd, Chichester, UK, 2012.

[12] AUEL, C., ALBAYRAK, I., SUMI, T., BOES, R.M. Sediment transport in high-speed flows over a fixed bed: 1. Particle dynamics. *Earth Surface Processes and Landforms*, DOI: 10.1002/esp.4128, 2017.

[13] AUEL, C., ALBAYRAK, I., SUMI, T., BOES, R.M. Sediment transport in high-speed flows over a fixed bed: 2. Particle impacts and abrasion prediction. *Earth Surface Processes and Landforms*, DOI: 10.1002/esp.4132, 2017.